On estimation of wind velocity, angle-of-attack and sideslip angle of small UAVs using standard sensors

Tor A. Johansen, Andrea Cristofaro, Kim Sørensen, Jakob M. Hansen, Thor I. Fossen

Abstract— **It is proposed to estimate wind velocity, Angle-Of-Attack (AOA) and Sideslip Angle (SSA) of a fixed-wing Unmanned Aerial Vehicle (UAV) using only kinematic relationships with a Kalman Filter (KF), avoiding the need to know aerodynamic models or other aircraft parameters. Assuming that measurements of airspeed and attitude of an UAV are available as inputs, a linear 4th order time-varying model of the UAV's longitudinal speed and the 3-D wind velocity is used to design a Kalman-filter driven by a GNSS velocity measurement airspeed sensor. An observability analysis shows that the states can be estimated along with an airspeed sensor calibration factor provided that the flight maneuvers are persistently exciting, i.e. the aircraft changes attitude. The theoretical analysis of the KF shows that global exponential stability of the estimation error is achieved under these conditions. The method is tested using experimental data from three different UAVs, using their legacy autopilot to provide basic estimates of UAV velocity and attitude. The results show that convergent estimates are achieved with typical flight patterns indicating that excitation resulting from the environment and normal flight operation is sufficient. Wind velocity estimates correlate well with observed winds at the ground. The validation of AOA and SSA estimates is preliminary, but indicate some degree of correlation between the AOA estimate and vertical accelerometer measurements, as would be expected since lift force can be modeled as a linear function of AOA in normal flight.**

I. INTRODUCTION

A fixed-wing aircraft's Angle-Of-Attack (AOA) and Side-Slip Angle (SSA) are important variables that contain useful information about the performance and safety of the aircraft in both normal and abnormal conditions. Larger aircrafts are usually equipped with vanes or multi-port air data probes that, when properly calibrated, can be used to infer the wind velocity, AOA and SSA. Small UAVs, on the other hand, does usually not have sensors dedicated to measurement of these variables due to their relatively large weight, size, cost and power consumption. In this paper we study conditions under which the AOA and SSA can be estimated using standard sensors without employing a model of the UAV dynamics (i.e. using only exact kinematic relationships). The standard sensor suite contains GNSS (Global Navigation Satellite System), IMU (Inertial Measurement Unit), and pitot-static tube.

A model-free approach is highly desirable since the estimates of AOA and SSA can then be used to directly detect faults and changes related to structural damage, icing, [1], and other adverse condition that might influence the aerodynamic coefficients or the UAV. It may also enable accurate control of small UAVs in agile maneuvers (e.g. [2]) with high AOA or SSA where aerodynamic models may be quite inaccurate since data from computational fluid dynamics or wind-tunnel tests may not be available for small low-cost UAVs, and calibration for payload weight distribution and other changes that may occur when the UAV is customized or modified between missions may be impractical or cumbersome. Finally, a model-free approach simplifies configuration since the method will be independent of the aircraft.

A commonly proposed estimation approach is the use of an Extended Kalman-Filter (EKF) based on the nonlinear kinematics and measurement model, possibly also in combination with an aerodynamic model, see [3], [4], [5], [6]. The method in [5] uses a similar sensor suite with GPS, IMU and pitot-static pressure sensor for wind velocity estimation, from which AOA and SSA can be derived without using an aerodynamic model. It estimates wind speed, its horizontal direction, and the airspeed sensor correction factor. Since the measurement model is nonlinear, an EKF is used for estimation. The method was used for airspeed sensor fault diagnosis in [7].

In [8], they propose a method which uses GPS/IMU sensors, but avoids the use of a pitot-

Centre for Autonomous Marine Operations and Systems, Department of Engineering Cybernetics, Norwegian University of Science and Technology, Trondheim, Norway

static pressure sensor due the use of a dynamic model of the aircraft. The method in [9] estimates wind velocity using only GPS/IMU sensors, but relies on circular maneuvers in the horizontal plane or a helical flight pattern. [10] proposes a modular architecture using GPS/IMU to calculate ground velocity, however uses an aerodynamic model to get an accurate estimation of AOA and SSA. Kinematic vehicle models together with GPS/INS and airspeed sensors are used in [11]. A wind velocity model is generated by differentiating the "wind-triangle" equations and used in a least-squares estimator. This requires that airspeed measurements are differentiated by taking differences between discrete samples. An EKF is proposed for estimation of wind velocities, SSA and AOA in [12]. The method applies a sensor suite with GPS/INS and pitot-static tube together with kinematic and dynamic models having known aerodynamic coefficients. Wind velocity estimation can also be made by measuring the relative motion of the UAV relative to the ground using a camera, [13].

The main contribution of the present paper is a model-free approach that does not include any aircraft-specific parameters, and at the same time can estimate the mean wind velocity in three dimensions, and the pitot-static tube correction factor in order to provide automatic online calibration and fault diagnosis of the airspeed sensor. Two types of airspeed sensors are considered: Pitot-static tubes that are fixed to the longitudinal axis of the UAV, and pitot-static tubes that are self-aligning with the air velocity vector. The dynamic observer model is a linear time-varying model that avoids linearization about the estimated state trajectory commonly employed when using an EKF as in [5]. As a consequence, it is shown that Global Exponential Stability (GES) of the estimator error dynamics can be achieved under an explicit persistence of excitation condition that requires maneuvers which change the aircraft attitude. Experimental results with three different UAVs having different autopilots and performing different maneuvers are included to illustrate that the method is independent of the aircraft, since exactly the same estimator parameters are used in all cases. Moreover, the experimental data illustrate how different maneuvers contribute to fulfillment of the persistence of excitation condition.

II. KINEMATICS

Let $\vec{v}_g$ denote the velocity vector of the aircraft relative to Earth, where the arrow means that it is a coordinate-free vector. Let $v_g^b = (u, v, w)^T$ contain its components decomposed in the aircraft's BODY coordinate frame, and $v_g^n = (u_g, v_g, w_g)^T$ contain its components decomposed in an Earth-fixed North-East-Down (NED) coordinate frame. The aircraft kinematics are now, [3]

$$\dot{u} - rv + qw = a_x \quad (1)$$

$$\dot{v} - pw + ru = a_y \quad (2)$$

$$\dot{w} - qu - pv = a_z \quad (3)$$

where the components of the UAV's acceleration vector $\vec{a}$ are decomposed in the BODY frame as $a^b = (a_x, a_y, a_z)^T$, and p, q, r are angular rates. Let the velocity vector of wind relative to Earth be $\vec{v}_w$ and $v_w^n = (u_w, v_w, w_w)^T$ denote its decomposition in the NED frame. The velocity of the aircraft relative to the wind velocity is then $\vec{v}_r = \vec{v}_g - \vec{v}_w$. The rotation matrix from NED to BODY is denoted R_n^b and is defined by the roll (ϕ), pitch (θ) and yaw (ψ) angles. Hence, the relative velocity $\vec{v}_r$, decomposed in the BODY frame as $v_r^b = (u_r, v_r, w_r)^T$, is, [3]

$$\begin{pmatrix} u_r \\ v_r \\ w_r \end{pmatrix} = \begin{pmatrix} u \\ v \\ w \end{pmatrix} - R_n^b \begin{pmatrix} u_w \\ v_w \\ w_w \end{pmatrix} \quad (4)$$

The sideslip angle β and the angle-of-attack α are the angles between the BODY-fixed axes of the aircraft and its relative velocity vector $\vec{v}_r$, [3]:

$$\alpha = \tan^{-1}(w_r/u_r) \quad (5)$$

$$\beta = \sin^{-1}(v_r/V_a) \quad (6)$$

and $V_a = \sqrt{u_r^2 + v_r^2 + w_r^2}$ is the airspeed.

III. SENSORS

Assume the following relatively standard sensor suite (e.g. [14]):

- GNSS providing measurements of velocity.
- AHRS (Attitude and Heading Reference System) providing measurements of roll, pitch and yaw. This is usually realized using an IMU providing measurements of specific force and angular velocity. In addition, GNSS velocity or magnetometer measurements may be used to give information about the heading.

- Pitot-static tube with differential pressure sensor providing measurement of u_r when it is fixed aligned with the longitudinal axis of the UAV, or V_a it it is self-aligning (which is not common on small UAV's).

IV. ESTIMATOR STRUCTURE

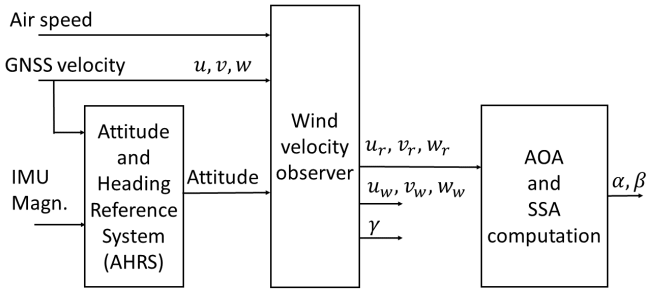

Fig. 1. Estimator structure.

The proposed estimator structure is illustrated in Figure 1. Since it is a cascade, its stability properties are inherited from the individual modules, [15]. It has the following modules

- AHRS estimating the attitude (roll, pitch and yaw angles ϕ, θ, ψ) based on (1)-(3). This could be based on the EKF, e.g. [3] or nonlinear observers with semi-global or global regions of attraction, e.g. [3], [14], [16], [17], [18].
- The "wind velocity observer" estimates the wind velocity based on (4), see section V where it is considered in detail, such that aircraft relative velocity can be input to the computation of AOA and SSA.
- The "AOA and SSA computation" module applies (5) and (6).

V. WIND VELOCITY OBSERVER

The estimation of wind velocity is non-trivial, since we need to make additional assumptions on the wind dynamics and UAV motion. We assume the wind is steady (slowly time-varying) relative to Earth

$$\dot{v}_w^n = 0 \tag{7}$$

This model will be used in a KF where the estimates will be predicted using this model (no change), and updated using measurements. This means that time-varying wind velocities can still be accurately estimated despite this assumption, since the gain of the KF effectively defines a filter cut-off frequency. Wind velocity frequencies that are slower than this cut-off frequency are estimated by the KF, while faster frequency components are filtered away from the estimate. Hence the KF gain should be optimally selected having both this and the sensors' noise levels in mind.

A. Longitudinal air speed sensor

Suppose $u_r = \gamma u_r^m$, wkere u_r^m is the measurement given by the airspeed sensor and γ is an unknown sensor scaling factor that will be estimated as an online calibration or fault diagnosis of the sensor. Hence, we use the following measurement equation for design of the observer injection term

$$u = d_1^T R_n^b v_w^n + u_r^m \gamma \tag{8}$$

where $d_1 = (1, 0, 0)^T$ and we assume u to be a measured output signal derived from the GNSS velocity and AHRS. We use the model

$$\dot{\gamma} = 0 \tag{9}$$

for the airspeed sensor scaling factor, assuming it is slowly time-varying. Defining the state $x = ((v_w^n)^T, \gamma)^T \in \mathbb{R}^4$, eq. (9) together with (7) and (8) leads to the system matrix $A = 0$ and the time-varying measurement matrix

$$C = (d_1^T R_n^b,\ u_r^m) \tag{10}$$

such that (8) can be written $u = Cx$. The observability Grammian is therefore

$$W_o(t_0, t_1) = \int_{t_0}^{t_1} \begin{bmatrix} (R_n^b)^T D R_n^b & u_r^m (R_n^b)^T d_1 \\ d_1^T R_n^b u_r^m & (u_r^m)^2 \end{bmatrix} dt$$

where

$$D = d_1 d_1^T = \begin{bmatrix} 1 & 0 & 0 \\ 0 & 0 & 0 \\ 0 & 0 & 0 \end{bmatrix}$$

First we note that for a fixed-wing UAV, we generally have $u_r^m \neq 0$. Due to $\text{rank}(D) = 1$, we depend on time-variations in the matrix R_n^b to achieve observability of the wind velocity, i.e. the UAV needs to make maneuvers with changes in attitude in order to satisfy a persistence of excitation (PE)

condition that is sufficient for uniform complete observability, [19], where there must exist a $T > 0$ and $\epsilon > 0$ such that for all $t > 0$ we have

$$W_o(t, t+T) \;\geq\; \epsilon I_4 \tag{11}$$

This is a quite intuitive condition, considering that the pitot-static tube measures the component of the wind velocity projected on its longitudinal axis that is usually aligned with the longitudinal axis of the UAV. In order to gather the information necessary to find all component of the wind velocity vector, it must probe in different directions. Flight at constant attitude gives rank$(W_o) = 2$ while some variations in pitch and yaw leads to rank$(W_o) = 4$.

Consider the observer

$$\begin{pmatrix} \dot{\hat{v}}_w^n \\ \dot{\hat{\gamma}} \end{pmatrix} \;=\; K\left(u - u_r^m\hat{\gamma} - d_1^T R_n^b \hat{v}_w^n\right) \tag{12}$$

with gain vector $K = (k_u, k_v, k_w, k_\gamma)^T \in \mathbb{R}^4$. The error $\tilde{x}_w^n = (v_w^n - \hat{v}_w^n; \gamma - \hat{\gamma})$ satisfies the Linear Time-Varying (LTV) dynamics

$$\dot{\tilde{x}} \;=\; KC\tilde{x} \tag{13}$$

A time-varying gain matrix K can be designed using $A = 0$ and the given C with the time-varying Kalman-Bucy filter, [19]:

$$K = PC^T R^{-1}, \quad \dot{P} = Q - PC^T R^{-1} CP \tag{14}$$

where $R > 0$ is the variance of the sensor noise on u, $Q > 0$ is the covariance of a white noise model of the wind velocity and scaling factor rates of change, and the initial condition is $P(0) > 0$, where both are symmetric matrices. We note that with the PE condition satisfied, this leads to bounded P and renders the observer GES, [20].

B. Self-adjusting air speed sensor

Suppose instead that V_a is measured by a self-adjusting airspeed sensor as $V_a = \gamma V_a^m = ||v_r^b||$, with an unknown scaling factor γ. Hence, we have the measurement equation

$$v_g^b = R_n^b v_w^n + v_r^b = R_n^b v_w^n + V_a^m \frac{v_r^b}{||v_r^b||}\gamma \tag{15}$$

and we can define the estimated measurement

$$\hat{v}_g^b \;=\; R_n^b \hat{v}_w^n + V_a^m d_1 \hat{\gamma} \tag{16}$$

and time-varying

$$C = (R_n^b, V_a^m d_1) \tag{17}$$

Using algebraic manipulation we get

$$v_g^b - \hat{v}_g^b \;=\; R_n^b \tilde{v}_w^n + \tilde{\gamma} V_a^m d_1 + V_a \tilde{d} \tag{18}$$

with $\tilde{d} = v_r^b/||v_r^b|| - d_1$ may be non-zero only due to non-zero AOA and SSA. Hence, we can design the observer

$$\begin{pmatrix} \dot{\hat{v}}_w^n \\ \dot{\hat{\gamma}} \end{pmatrix} = K(v_g^b - R_n^b \hat{v}_w^n + V_a^m d_1)\hat{\gamma} \tag{19}$$

and get the error dynamics

$$\dot{\tilde{x}} \;=\; KC\tilde{x} + e \tag{20}$$

where $e = KV_a\tilde{d}$ is easily seen to be bounded. We also have $A = 0$ and use the same equations for the KF as before, but with the C-matrix (17) and appropriate covariance matrices. The origin of the nominal error dynamics $\tilde{x}$ is GES when $e = 0$ and a PE condition is satisfied, and the error converges to a ball centered at the origin when $e \neq 0$. We note that the PE condition is derived as above, and only slightly different with small AOA and SSA since $\tilde{d} \approx 0$.

VI. Aerodynamic forces

The specific force measurements in the BODY coordinate frame are directly given by the IMU's accelerometers [3]:

$$f_x \;=\; a_x + g\sin(\theta) \tag{21}$$
$$f_y \;=\; a_y - g\sin(\phi)\cos(\theta) \tag{22}$$
$$f_z \;=\; a_z - g\cos(\phi)\cos(\theta) \tag{23}$$

where g is the gravity constant. The specific force vector in the BODY frame equals to the sum of the aerodynamic forces on the UAV, [3]:

$$f_x \;=\; \frac{1}{m}(F_{ax} + F_T) \tag{24}$$
$$f_y \;=\; \frac{1}{m}F_{ay} \tag{25}$$
$$f_z \;=\; \frac{1}{m}F_{az} \tag{26}$$

where $(F_{ax}, F_{ay}, F_{az})^T$ are aerodynamic forces represented as a vector decomposed in the BODY frame, m is mass, and F_T is the magnitude of the propulsion force that is assumed to be aligned with the longitudinal BODY axis.

The aerodynamic force models are relationships between α, β, V_a and the propeller angular speed

Fig. 2. The UAV's used for testing. From top: Penguin B, Sierra and X8.

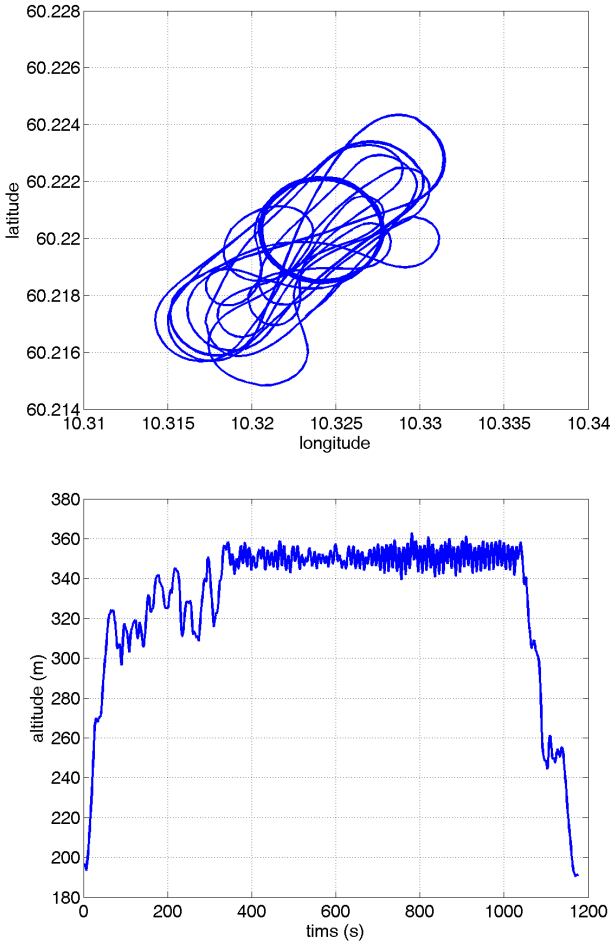

Fig. 3. Flight path. Penguin B UAV, using Piccolo SL sensors telemetry log.

ω_p on one side, and the aerodynamic forces are given by, [3]:

$$F_{ax} = \frac{1}{2}\varrho V_a^2 S C_X(\alpha) \quad (27)$$

$$F_{ay} = \frac{1}{2}\varrho V_a^2 S C_Y(\beta) \quad (28)$$

$$F_{az} = \frac{1}{2}\varrho V_a^2 S C_Z(\alpha) \quad (29)$$

$$F_T = \frac{1}{2}\varrho S_{prop} C_{prop}(k_p^2\omega_p^2 - V_a^2) \quad (30)$$

where S is the planform area of the wing, ϱ is the air mass density, and the lift and drag coefficients are defined as a function of α as follows

$$C_X(\alpha) = C_L(\alpha)\sin(\alpha) - C_D(\alpha)\cos(\alpha) \quad (31)$$

$$C_Z(\alpha) = -C_L(\alpha)\cos(\alpha) - C_D(\alpha)\sin(\alpha) \quad (32)$$

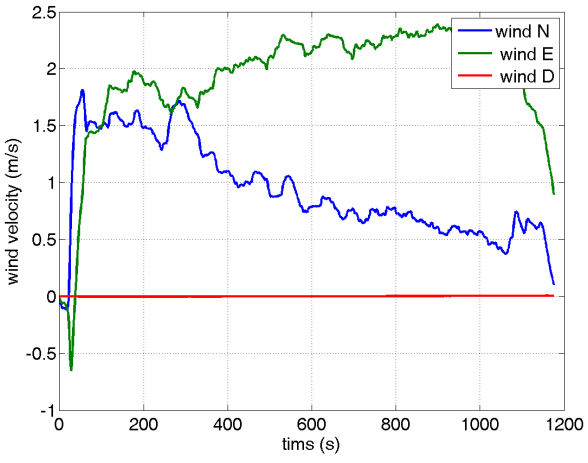

Fig. 4. Estimated wind velocity. Penguin B UAV, using Piccolo SL sensors telemetry log.

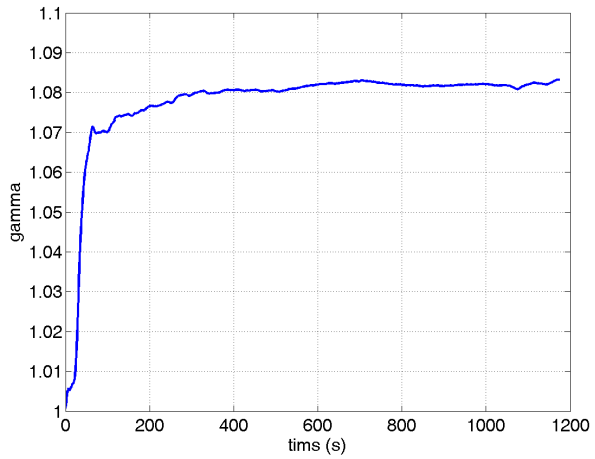

Fig. 5. Estimated pitot tube scaling factor. Penguin B UAV, using Piccolo SL sensors telemetry log.

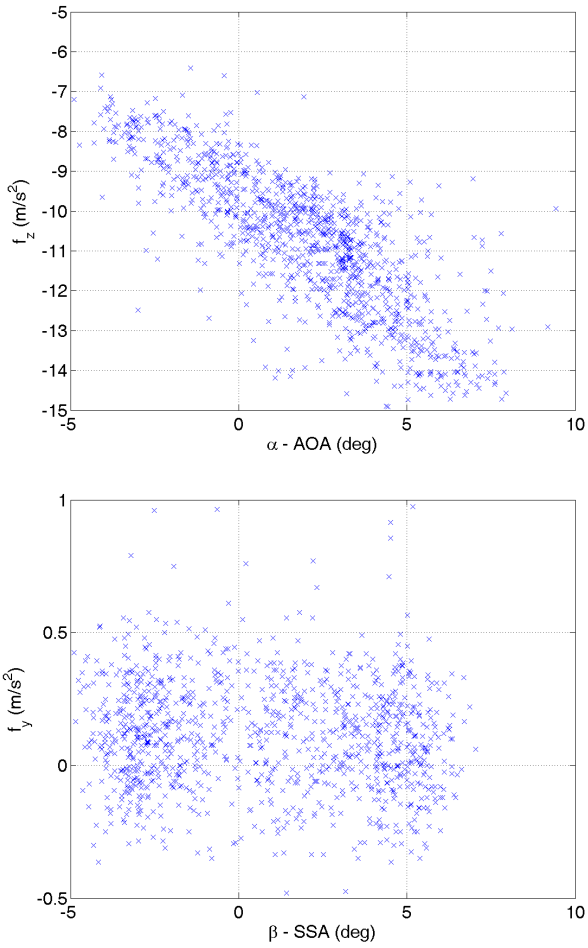

Fig. 6. AOA and SSA correlations. Penguin B UAV, using Piccolo SL sensor telemetry log.

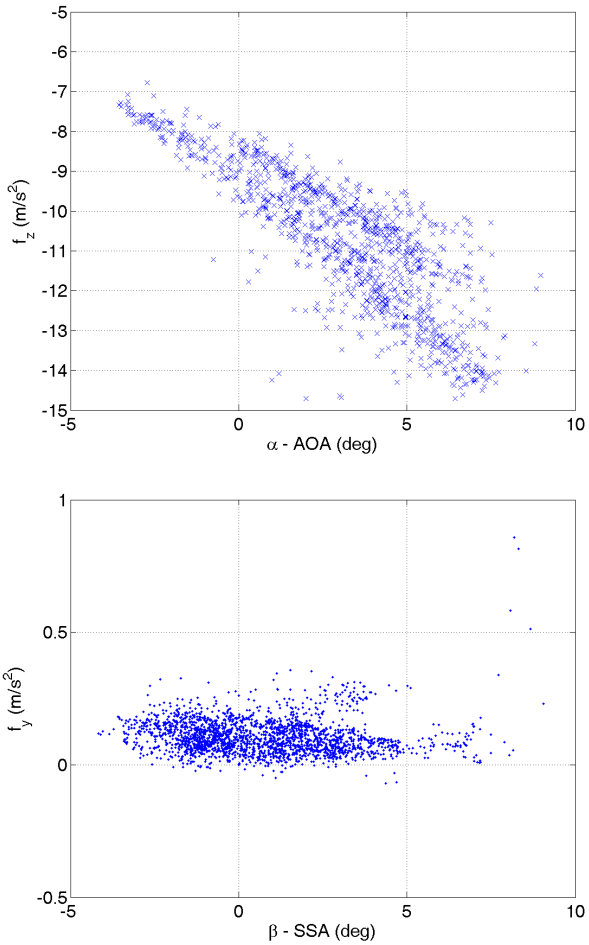

Fig. 7. AOA and SSA correlations. Penguin B UAV, using reference sensor system high-frequency log.

VII. EXPERIMENTAL TEST RESULTS

All tests uses off-the-shelf autopilots with an AHRS and GPS to provide velocity and attitude estimates as input to the estimation algorithm (12), which is implemented as a discrete-time Kalman-filter with $R = 1$ and

$$\begin{aligned} P(0) &= \text{diag}(10^{-2}, 10^{-2}, 10^{-6}, 10^{-4}) \\ Q &= \text{diag}(10^{-3}, 10^{-3}, 10^{-6}, 10^{-8}) \end{aligned}$$

Exactly the same tuning parameters are used for all tests involving the three different UAVs shown in Figure 2. Initial conditions at $t = 0$ are $\hat{\gamma}(0) = 1$ and $\hat{v}_w^n = (0, 0, 0)$.

A. NTNU Penguin, Eggemoen, 4 Nov 2014

The Penguin B UAV (GTOW about 20 kg) with Piccolo SL autopilot was used. The flight

duration is about 20 minutes with takeoff, circles and figure-8-loops at about 500 ft altitude above ground, before landing. Due to some issues the pitch oscillates with a 10 second period during the level flight period, leading to variations in altitude up to 20 meters. Airspeed varies slightly around 30 m/s. The data are logged by the autopilot over the radio telemetry link at 1 second intervals.

Figures 3-5 show the test results. At Eggemoen the winds are estimated to about 2 m/s, which is consistent with weather observations and data from `http://yr.no` at the time. There is a scale factor error of about $8\ \%$ on the air speed sensor, which is quickly identified by the estimator already during the climb after takeoff.

The observability Gramian (with T equal to the full length of the data set, and scaled) is given by

$$W_o = \begin{bmatrix} 263.4 & 90.2 & -1.6 & 807.0 \\ 90.2 & 264.1 & 0.268 & 892.4 \\ -1.6 & 0.268 & 3.6 & 285.9 \\ 807.0 & 892.4 & 285.9 & 393 \cdot 10^3 \end{bmatrix}$$

We note that the estimate of the z-component of v_w^n is more uncertain than the x, y-components, which is expected since there are larger variations in yaw than pitch.

Consider the UAV's body z-axis and eqs. (26), (29) and (32). For small AOA they lead to the following approximation

$$f_z \;=\; k_0 + k_1\alpha \tag{33}$$

for some parameters k_0 and k_1 that depend on airspeed, the rotational velocity q, and elevator control action, cf. p. 49 in [3]. Notice that a non-zero k_0 typically results from an offset between the UAV's longitudinal body axis and the airfoil's chord line. In order to validate the estimates of AOA, we can investigate if they are consistent with (29). The upper part of Figure 6 shows the estimated AOA (α) plotted versus the specific force f_z measured by the IMU. We see that there is a linear correlation between f_z and α as expected. We note that the slope is negative due to the positive z-axis pointing downwards.

A linear correlation can be expected also for small SSA, cf. p. 50 in [3]

$$f_y \;=\; \kappa_0 + \kappa_1\beta \tag{34}$$

for some parameters κ_0 and κ_1, where κ_0 depends on airspeed, aileron and rudder control forces, and angular velocities p and r. The data in the bottom part of Figure 6 is, however, not able to clearly identify a significant correlation.

For reference, the same variables are estimates using a different set of sensors installed on the UAV during the same flights. This sensor suite consists of a uBlox LEA-6T GPS receiver producing both pseudo-range and carrier-phase measurements at 5 Hz that were processed using RTKLIB and data from a local base station in order to generate high quality Real-Time Kinematics (RTK) measurements. It also consists of an ADIS IMU operating at 410 Hz, that was used to produce integrated GPS/INS estimates of attitude and velocity using a nonlinear observer, [16]. Air speed data with a sampling frequency of 1 Hz from Piccolo was used. Digital low-pass filtering at 410 Hz sampling frequency was applied to reduce the effects of high-frequency vibrations from the combustion engine. The estimates appears to have slightly stronger correlations for AOA and significantly better correlations for SSA than the ones achieved by the Piccolo sensor suite, as illustrated in Figure 7 that shows the estimated values.

Careful study of the data have suggested that the remaining errors are likely due to the dependence on airspeed, angular velocities and control actions, as well as smaller errors and phase delays in attitude estimates, inaccuracies in time-synchronization of the measurements due to latencies in the GPS velocity measurements, and undetected high-frequency wind-induced motions.

B. NASA Sierra, Svalbard, 18 Jul 2009 about 10:30

The NASA Sierra UAV (GTOW about 200 kg) with Piccolo autopilot was used. The test data set contains about 100 minutes of flight, with a take-off, some figure-8-loops before the UAV follows three straight legs of its mission path. The first part is at 1000 ft altitude above mean sea level, while the last part is at 600 ft altitude. Data are logged over Iridium telemetry at typically 3 second intervals, with frequent data dropouts.

Estimates and experimental data are shown in Figures 8-11. The winds are estimated to be about 10 m/s, which is consistent with the autopilot's own estimates. Weather data from `http://yr.no` reports winds of 8 m/s at 11:00 to 10.5 m/s at 14:00 at the ground.

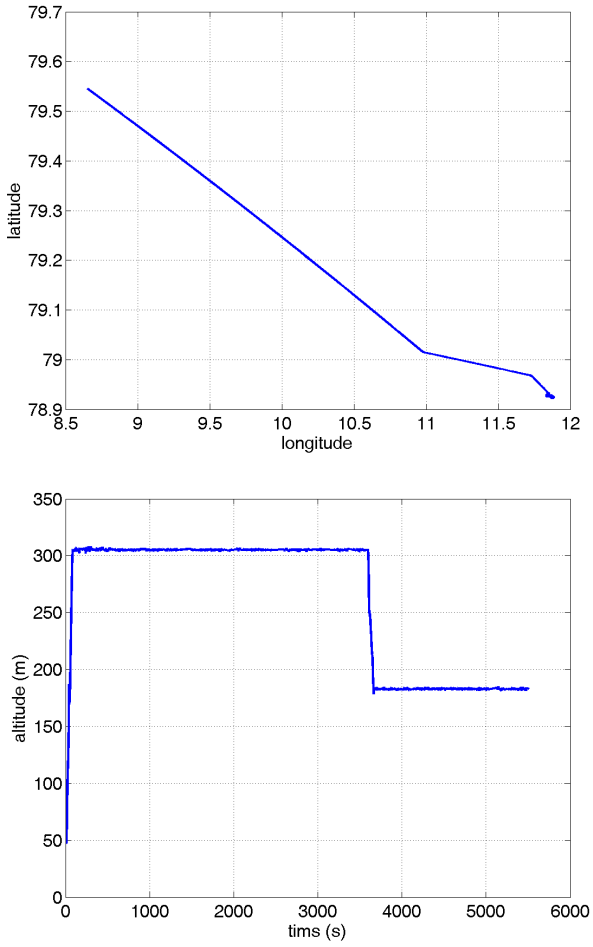

Fig. 8. Flight path. NASA Sierra, using Piccolo sensor telemetry (Iridium).

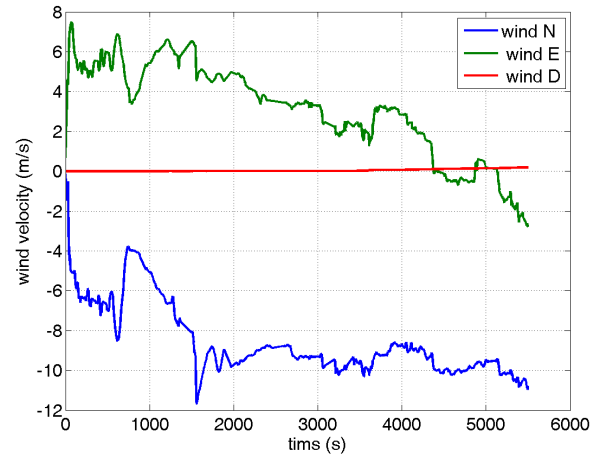

Fig. 9. Estimated wind velocity. NASA Sierra, using Piccolo sensor telemetry (Iridium).

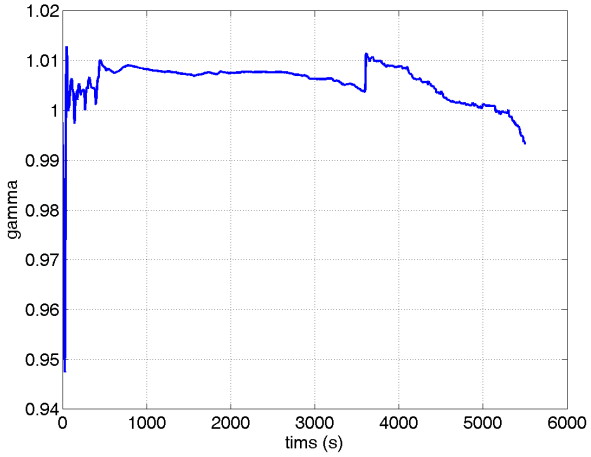

Fig. 10. Estimated pitot-tube scaling factor. NASA Sierra, using Piccolo sensor telemetry (Iridium).

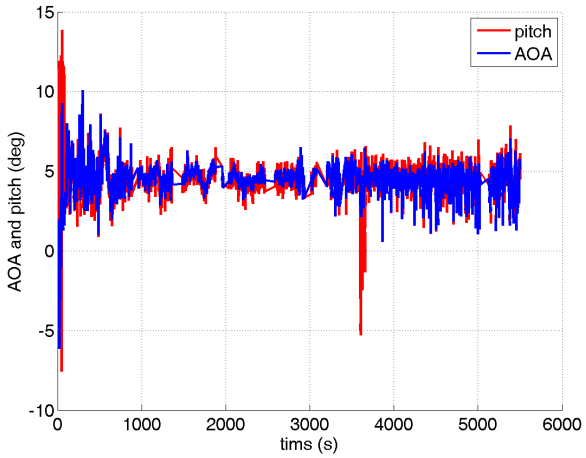

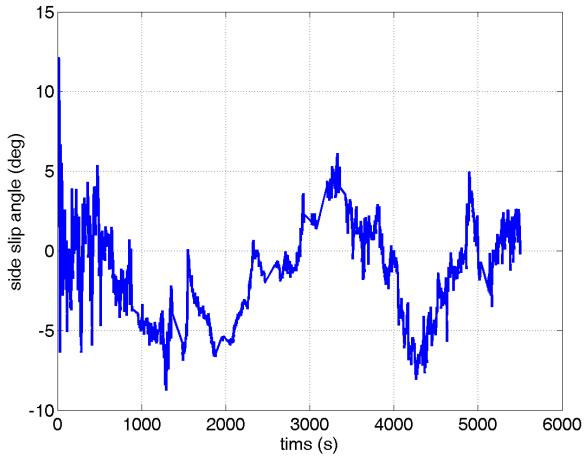

Fig. 11. Estimated AOA, pitch and SSA angles. NASA Sierra, using Piccolo sensor telemetry (Iridium).

We note the initial dip in the estimate of γ. This seems to be due to some latency or filtering in the GPS receiver or autopilot as the estimate responds more slowly than the airspeed sensor during the takeoff. Due to heavy cross track winds, the SSA is estimated to vary between -5 and +5 deg during most of the flight. AOA is estimated to approximately 5 deg during steady flight.

C. NTNU X8 UAV, 15 May 2014, Hopavågen about 13:30

A Skywalker X8 flying-wing UAV (GTOW about 4 kg) with APM 2.5 autopilot was used. The flight lasts about 20 minutes with a take-off, loitering over a target, and then landing. The UAV was operated manually with RC (remote control) in order to manage highly unsteady winds and turbulence that were caused by operating close to mountains in a coastal environment. Data were logged at irregular intervals (typically 5 times per second) by the Mission Planner through telemetry data received over a wireless network link.

Test flight data and results are given in Figures 12-14. The airspeed sensor scaling factor was estimated to approximately 1.7, indicating that it was highly uncalibrated.

VIII. DISCUSSION AND CONCLUSION

It is studied how to estimate wind velocity, AOA and SSA using only kinematic relationships, avoiding the need to know aerodynamic models or other aircraft parameters. The paper investigates conditions under which these variables are possible to estimate. Assuming slowly varying winds, and a sensor suite consisting of GNSS, IMU and a pitot-static tube as a minimum configuration, it is shown that these variables can be estimated along with an airspeed sensor calibration factor, provided the aircraft changes pitch and yaw. The theoretical analysis shows global exponential stability of the estimation error dynamics.

The method is tested using experimental data from three different UAVs, using their off-the-shelf autopilot to provide estimates of UAV velocity and attitude. The flight conditions contain low and high winds, steady and turbulent winds, climbs, descents, straight paths, small course changes, and loops. The results show that convergent estimates are achieved with all these typical flight patterns

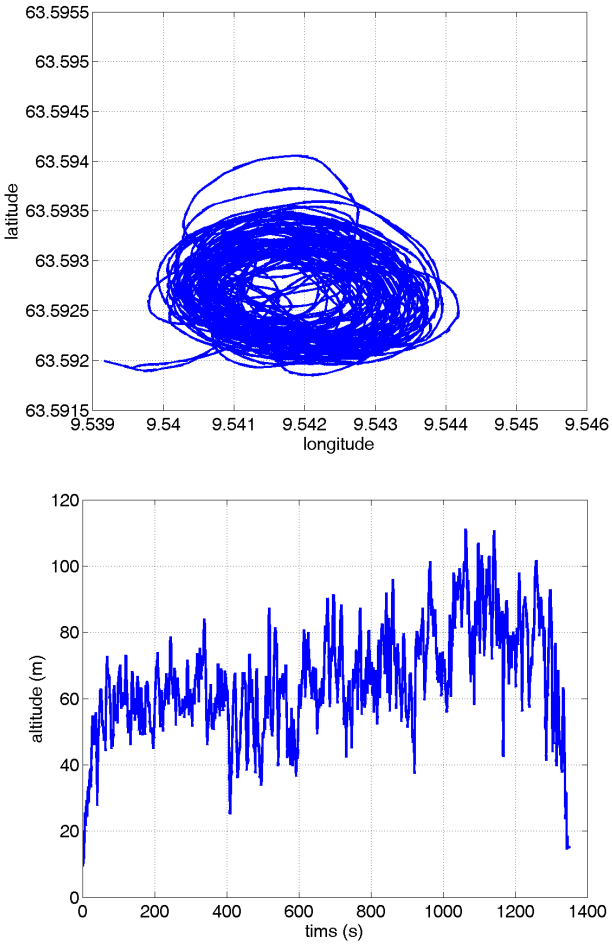

Fig. 12. X8 UAV, using Ardupilot 2.5 sensor telemetry log.

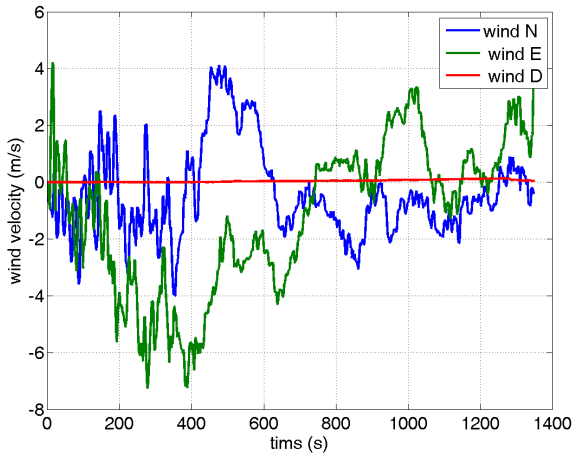

Fig. 13. X8 UAV, using Ardupilot 2.5 sensor telemetry log.

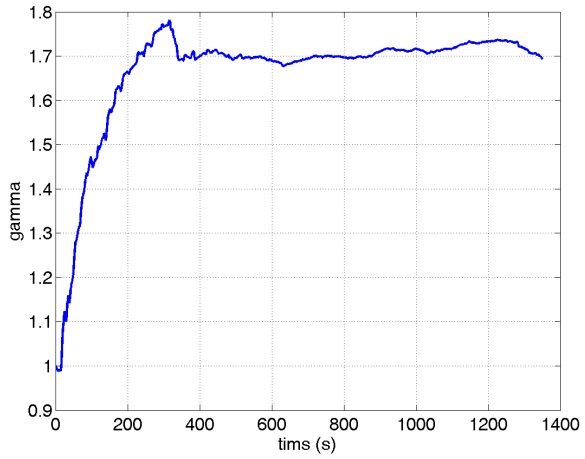

Fig. 14. X8 UAV, using Ardupilot 2.5 sensor telemetry log.

indicating that excitation resulting from the environment and flight operation is sufficient. The estimated AOA and SSA are to some extent correlated with the expected values under the prevailing flight conditions, although we cannot conclude about the accuracy of the estimates due to the lack of a direct measurement of the true values for validation. The results are therefore considered as preliminary, and future work will focus on validation of the accuracy of the method in various conditions.

ACKNOWLEDGMENTS

This work has been carried out at the Centre for Autonomous Marine Operations and Systems (AMOS), supported by the Research Council of Norway through the Centres of Excellence funding scheme, project number 223254, and the FRINATEK project 221666.

We are grateful to NASA Ames, and Dr. Matt Fladeland in particular, for providing flight data, and the UAV pilots Lars Semb and Torkel Hansen at NTNU, and Carl-Erik Stephansen at Maritime Robotics AS, for assistance with flight tests. We also thank Nadia Sokolova for expertize on GNSS.

REFERENCES

[1] K. L. Sørensen, M. Blanke, and T. A. Johansen, "Diagnosis of wing icing through lift and drag coefficient change detection for small unmanned aircraft," in *Proc. 9th IFAC Symposium on Fault Detection, Supervision and Safety of Technical Processes, Paris*, 2015.

[2] S. H. Mathisen, T. I. Fossen, and T. A. Johansen, "Non-linear model predictive control for guidance of a fixed-wing uav in precision deep stall landing," in *International Conference on Unmanned Aircraft Systems, Denver*, 2015.

[3] R. W. Beard and T. W. McLain, *Small Unmanned Aircraft: Theory and Practice*, 2012.

[4] C. Ramprasadh and H. Arya, "Multi-stage fusion algorithm for estimation of aerodynamic angles in mini aerial vehicle," in *Proc. 49th AIAA Aerospace Science Meeting, Orlando, FL*, 2011.

[5] A. Cho, J. Kim, S. Lee, and C. Kee, "Wind estimation and airspeed calibration using a UAV with a single-antenna GPS receiver and pitot tube," *IEEE Trans. Aerospace and Electronic Systems*, vol. 47, pp. 109–117, 2011.

[6] A. Cho, Y.-S. Kang, B.-J. Park, and C.-S. Yoo, "Airflow angle and wind estimation using GPS/INS navigation data and airspeed," in *Proc. 13th Int. Conf. Control, Automation and Systems (ICCAS), Gwangju, Korea*, 2013.

[7] S. Hansen and M. Blanke, "Diagnosis of airspeed measurement faults for unmanned aerial vehicles," *IEEE Trans. Aerospace and Electronic Systems*, vol. 50, pp. 224–239, 2014.

[8] P. A. P. Lie and D. Gebre-Egziabher, "Synthetc air data system," *J. Aircraft*, vol. 50, pp. 1234–1249, 2013.

[9] S. Mayer, G. Hattenberger, P. Brisset, M. O. Jonassen, and J. Reuder, "A 'no-flow-sensor' wind estimation algorithm for unmanned aerial systems," *Int. J. Micro Air Vehicles*, vol. 4, no. 1, pp. 15–29, 2012.

[10] H. Long and S. Song, "Method of estimating angle-of-attack and sideslip angle based on data fusion," in *Proc. Int. Conf. Intelligent Computation Technology and Automation*, 2009, pp. 641–644.

[11] J. W. Langelaan, N. Alley, and J. Neidhoefer, "Wind field estimation for small unmanned aerial vehicles," *J. Guidance, Control and Dynamics*, vol. 34, pp. 1016–1030, 2011.

[12] S. Leutenegger, A. Melzer, K. Alexis, and R. Siegwart, "Robust state estimation for small unmanned airplanes," in *Proc. IEEE Int. Conf. Control Applications, Antibes, France*, 2014, pp. 1003–1010.

[13] D. Zachariah and M. Jansson, "Self-motion and wind velocity estimation for small-scale UAVs," in *Proc. IEEE Int. Conf. Robotics and Automation, Shanghai*, 2011.

[14] D. B. Kingston and R. W. Beard, "Real-time attitude and position estimation for small UAVs using low-cost sensors," in *AIAA Conf.*, 2004.

[15] A. Loria and E. Panteley, "Cascaded nonlinear time-varying systems: analysis and design," in *Advanced Topics in Control Systems Theory*, F. Lamnabhi-Lagarrigue, A. Loria, and E. Panteley, Eds. Springer-Verlag, London, 2004, ch. 2.

[16] H. F. Grip, T. I. Fossen, T. A. Johansen, and A. Saberi, "Nonlinear observer for GNSS-aided inertial navigation with quaternion-based attitude estimation," in *Proc. American Control Conference, Washington DC*, 2013.

[17] ——, "Attitude estimation using biased gyro and vector measurements with time-varying reference vectors," *IEEE Trans. Automatic Control*, vol. 57, pp. 1332–1338, 2012.

[18] M.-D. Hua, F. Ducard, T. Hamel, R. Mahony, and K. Rudin, "Implementation of a nonlinear attitude estimator for aerial robotic vehicles," *IEEE Transactions on Control Systems Technology*, vol. 22, pp. 201–213, 2014.

[19] R. E. Kalman and R. S. Bucy, "New results in linear filtering and prediction theory," *Trans. ASME, Ser. D, J. Basic Eng*, pp. 95–109, March 1961.

[20] B. D. O. Anderson, "Stability properties of Kalman-Bucy filters," *J. Franklin Institute*, vol. 291, pp. 137–144, 1971.